

An analytical model for inelastic cyclic response of eccentrically braced frame with vertical shear link (V-EBF)



Jack Bouwkamp^a, Mohamad Ghasem Vetr^b, Ali Ghamari^{c,*}

^a Darmstadt University of Technology, Darmstadt, Germany

^b International Institute of Earthquake Engineering and Seismology (IIEES), Tehran, Iran

^c Department of Civil Eng. Darehshahr branch, Islamic Azad University, Ilam, Iran

ARTICLE INFO

Article history:

Received 26 November 2015

Received in revised form 3 May 2016

Accepted 5 May 2016

Available online 13 May 2016

Keyword:

V-EBF

Analytical

Hysteresis

Ductility

Strain hardening

Shear damper

ABSTRACT

Eccentrically Braced Frames (EBFs) have a capability of energy dissipation relying on horizontal link beams in main frame. Use of vertical link (V-EBF) enhances system performance; main frame damaged, easy replaces after earthquake, and it can be rehabilitated minor changes of existing structure. This paper describes experimental and analytical study of the V-EBF system. Experimental results showed that ultimate shear strength of vertical link is more than two times of yielding strength. In analytical model, Kinematic-Isotropic strain hardening for shear, and only Kinematic for moment, showed accurate results with an upper bound for yielding surface to the vertical link.

© 2016 The Author(s). Published by Elsevier Ltd. This is an open access article under the CC BY-NC-ND license (<http://creativecommons.org/licenses/by-nc-nd/4.0/>).

1. Introduction

Eccentrically Braced Frames (EBFs) have been used as a seismic load resisting system, primarily in buildings. This system, which relies on the yielding of a horizontal link beam between eccentric braces, has been shown to provide ductility and energy dissipation under seismic loading, and its behavior in various configurations has been investigated [1–12]. Despite high seismic energy dissipation, Horizontal EBF (H-EBF) has substantial disadvantages. In addition, in industrial structures such as power plants, deep beams are sometimes used to carry heavy loads and highly sensitive equipment. In these cases, to ensure that equipment works accuracy, load-bearing members such as beams and columns should remain in the elastic range as much as possible. Therefore, the use of horizontal link beams is not convenient. To overcome the problems in the EBF system, a new system called V-EBF (Vertical-EBF) was proposed [13]. In this system, reversed-V braces are attached to the beam with a shear panel. Intensive inelastic deformations are localized in the shear panel and the internal energy is dissipated by this member. Since all inelastic deformation is localized in the shear panel, there is no damage to the main members, also repairing after a strong earthquake is easier than H-EBF systems. Using the vertical links for seismic rehabilitation of the existing buildings is possible with minor changes in the main structure [14,15]. The Shear Panel System (SPS) is one of the simplest and cheapest passive energy dampers. The seismic performance improvement of bridges and towers with SPS systems was investigated [16–19]. Because of the effect of the shear panel on the behavior of V-EBF braces as a lateral load resisting system, improvement of shear panel performance is very important. Several studies have been conducted on this

* Corresponding author.

E-mail addresses: vetr@iiees.ac.ir (M.G. Vetr), aghamari@cmps2.iust.ac.ir (A. Ghamari).

system to prevent buckling the brace [20,21]. The results showed that with proper design, out-of-buckling do not occur in the vertical links of V-EBF systems.

In the present study, the cyclic behavior of the V-EBF system was evaluated experimentally and theoretically. Desirable performance of link beam in shear yielding (short link) than bending yielding has been shown in previous reports by researches, therefore, the short link without out-of-plane buckling are evaluated. Mathematical models are formulated to predict elastic and inelastic behavior. Also, adequate suggestions are presented to design of the V-EBF based on experimental results. Also, the presented suggestion are calibrated by numerical results.

2. Design of shear link

2.1. Horizontal shear link

The link is designed to act as a fuse by yielding and dissipating energy while preventing buckling of the brace members. The inelastic response of a link is strongly influenced by the link length and the M_p/V_p ratio of the link cross-section. Using plastic analysis, the plastic shear strength, V_p , and plastic moment strength, M_p , can be written as:

$$V_p = \frac{F_{yw}}{\sqrt{3}} \times t_w (d - 2t_f) \quad (1)$$

$$M_p = F_{yf} t_f (b - t_w) \times (d - t_f) + \frac{F_{yw} t_w d^2}{4} \quad (2)$$

where F_{yw} , F_{yf} are the web and flange yield strength, respectively, d is the overall beam depth, and t_f is the flange thickness, t_w is the web thickness, and b is the flange width.

Previous investigations [1–12] have shown that horizontal beam shear-link (the link length is designed to allow shear yielding without buckling of the web) possess excellent ductile behavior, and energy-dissipating capability. In fact, high isotropic strain hardening effects and combined bending and shear could be observed. They lead to increasing plastic-moment and shear capacities. In the ultimate state the shear and bending moment capacities reached values of about 1.5 V_p and 1.2 M_p , respectively. In order to impose shear yielding before bending yielding of the horizontal link, the link length e needs to be limited [9,22] to:

$$e \leq \frac{2 \times 1.2 M_p}{1.5 V_p} = 1.6 \frac{M_p}{V_p} \quad (3)$$

In other word, classification is based on the normalized link length, ρ , defined as; $\rho = \frac{V_p \times e}{M_p}$.

Capacity design approach is followed in an attempt to confine inelastic behavior to the shear links while all other frame members are designed to behave elastically.

According to AISC Seismic Provision [23] the links with $e \leq 1.6 \frac{M_p}{V_p}$ or $\rho \leq 1.6$ are shear links that yield predominantly in shear and have a maximum link rotation under the design seismic loading of 0.08 rad. The drift angle of the frame, θ , can then be written in terms of the link rotation angle, γ , as (See Fig. 1):

$$\theta_p = \gamma_p \frac{e}{L} \quad (4)$$

There are differences between the horizontal and vertical shear links. So, the equations about the calculation of the link rotation should be modified (See Fig. 2).

Also, when the link with length e deforms inelastically and resists against the applied base shear, the framing outside the link is designed to remain elastic. The elements outside the link are designed to resist against the forces generated by the fully yielded and strain hardened link. For short links ($\rho \leq 1.6$), the generated forces can be calculated as [22]: Link shear = 1.25 $R_y V_p$, Link end moment at beam = $R_y V_p$, Link end moment at brace = $[1.25 R_y V_p \times e - R_y M_p] \geq 0.75 R_y M_p$.

Where R_y is the ratio of the expected yield strength to the minimum specified yield strength F_y prescribed in AISC Seismic Provisions. The shear strength is increased by 1.25 to account strain hardening. Based on results of 16 links made from A992 steel, the average strain hardening ratio was formed to be 1.28, with a variation ranging from 1.17 to 1.44 [24]. Past researchers [9] have generally recommended a link over-strength factor of 1.5.

In order the element outside the link are designed to resist the forces generated by the fully yielded and strain hardened link. For short links ($\rho \leq 1.6$), the generated forces can be calculated as [22]:

In the following section, the equation for designing of the vertical shear link and structural elements outside the shear like are derived from experimental test. So, the generated forces factor is modified according to strain hardening results of vertical shear link. To design the V-EBF an analytical model is required.

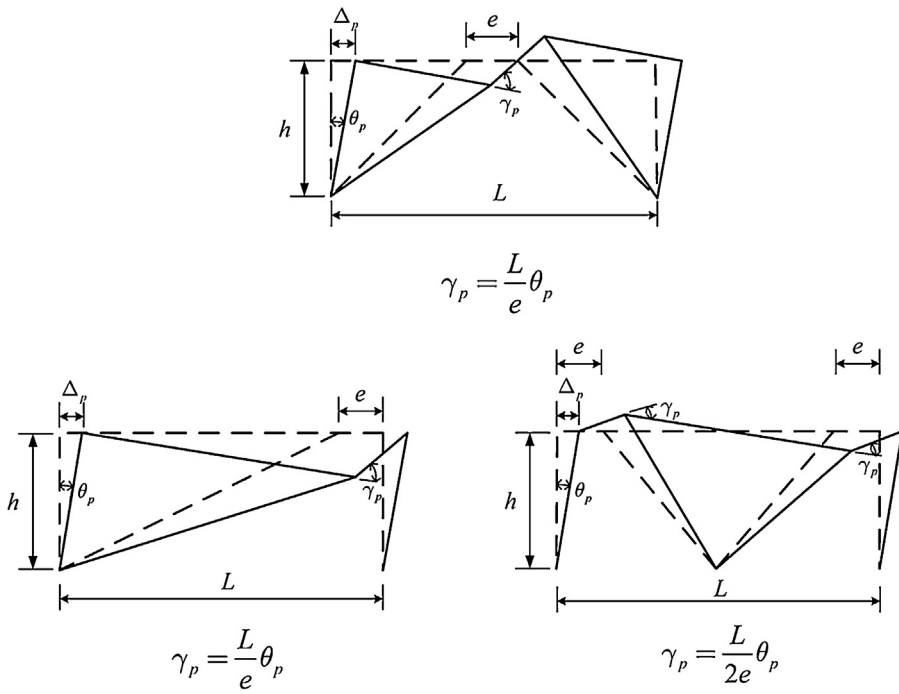


Fig. 1. Rotation of horizontal EBF [22].

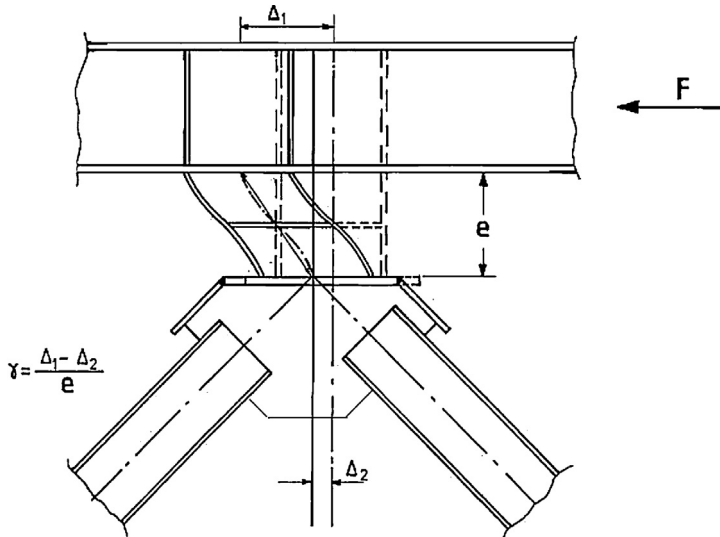


Fig. 2. Rotation of vertical shear link.

3. Analytical model of inelastic shear link element

3.1. General

It is necessary to develop an analytical model to determine the cyclic response of the V-EBF to compare the experimental results with numerically derived values. This analytical model must be able to take into account the nonlinear cyclic response of the plasticized element. It was noted previously sections, EBF inelastic behavior is confined on the shear link element. Therefore, an accurate model of the shear link element is necessary for numerical analysis that must be able to consider shear or moment capacities with strain hardening at any stage of the loading. Since the active links are subjected to large shear forces and bending moment, related formulation must include shear and bending effects on the elastic and inelastic states.

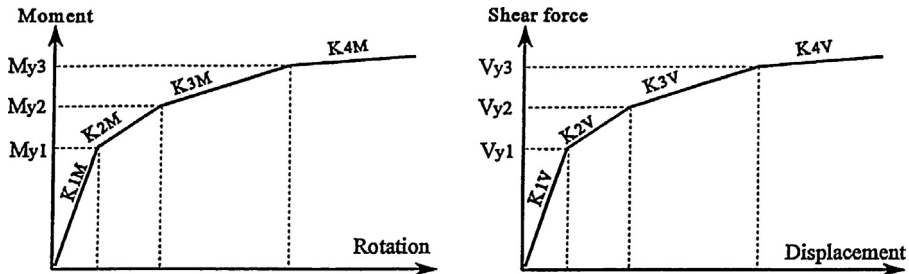


Fig. 3. Load (shear or moment) versus deflection (rotation or drift ratio) relationships.

3.2. Cyclic inelastic shear link model

Vertical or horizontal links are subjected to high levels of shear forces and bending moments in the active link regions. In the analysis of the link performance, elastic and inelastic deformations of both shear and flexural behaviors have to be taken into account. Some researchers have attempted to develop link models for the dynamic inelastic analysis of EBFs [10,25]. They modeled the link as a linear beam element with six nonlinear rotational and translational springs at each end. Three rotational and translational multilinear springs have been used to represent the flexural and shear inelastic behavior of the plastic hinge at the link end represented by the multilinear function shown in Fig. 3. The moment–rotation and the shear force–lateral displacement relationships of the shear link are shown in Fig. 3 is given as [10,25]:

(1) For shear (V values) and moment (M values):

$$V_{y1} = 1.00V_y \quad M_{\gamma 1} = 1.00M_y$$

$$V_{y2} = 1.06V_y \quad M_{\gamma 1} = 1.03M_y$$

$$V_{y3} = 1.12V_y \quad M_{\gamma 3} = 1.06M_y$$

(2) The values of K_2 , K_3 , K_4 for shear and moment are given relative to K_1 as follows:

$$K_{V2} = 0.030K_{V1} \quad K_{M2} = 0.030K_{M1}$$

$$K_{V3} = 0.015K_{V1} \quad K_{M1} = 0.015K_{M1}$$

$$K_{V4} = 0.002K_{V1} \quad K_{M3} = 0.002K_{M1}$$

where

$$K_{M1} = \frac{3EI}{e}; \quad K_{V1} = \frac{GA_w}{e}$$

In the above formulas, the shear and moment values present start of the web shear yielding and flanges yielding.

3.3. Strain hardening

Several researchers, [7,8,10,11] observed that during tests of shear links both isotropic and kinematic hardenings occur in such links that yield predominantly in shear. Based on experimental evidence, Ricles and Popov [10,11] concluded that the subhinges should follow an anisotropic hardening rule. In this rule, shear yielding follows a modified isotropic hardening rule while moment yielding obeys only a kinematic hardening rule. After initial yielding occurs, the behavior of a subhinge assumed to obey the Mroz [26,27] strain hardening assumptions for yielding in metals. On this basis, the yield function of an active link element is written as:

$$\Phi [S, \alpha, H(\varepsilon)] = 1 \quad (5)$$

where α is the vector of translation direction, $H(\varepsilon)$ is the isotropic expansion of the yield surface as a function of (ε) , in which ε is a scalar parameter monotonically increasing in the course of cyclic plastic shear flow, Fig. 4.

Considering the anisotropic rule, that assumes Isotropic and Kinematic hardening in shear yielding, and only Kinematic hardening for moment yielding, the yield function for the two cases become:

$$\Phi [M_z - \alpha_{Mz}] = 1 \quad (6)$$

$$\Phi [V_y - \alpha_{V_y}] = H(\varepsilon) \quad (7)$$

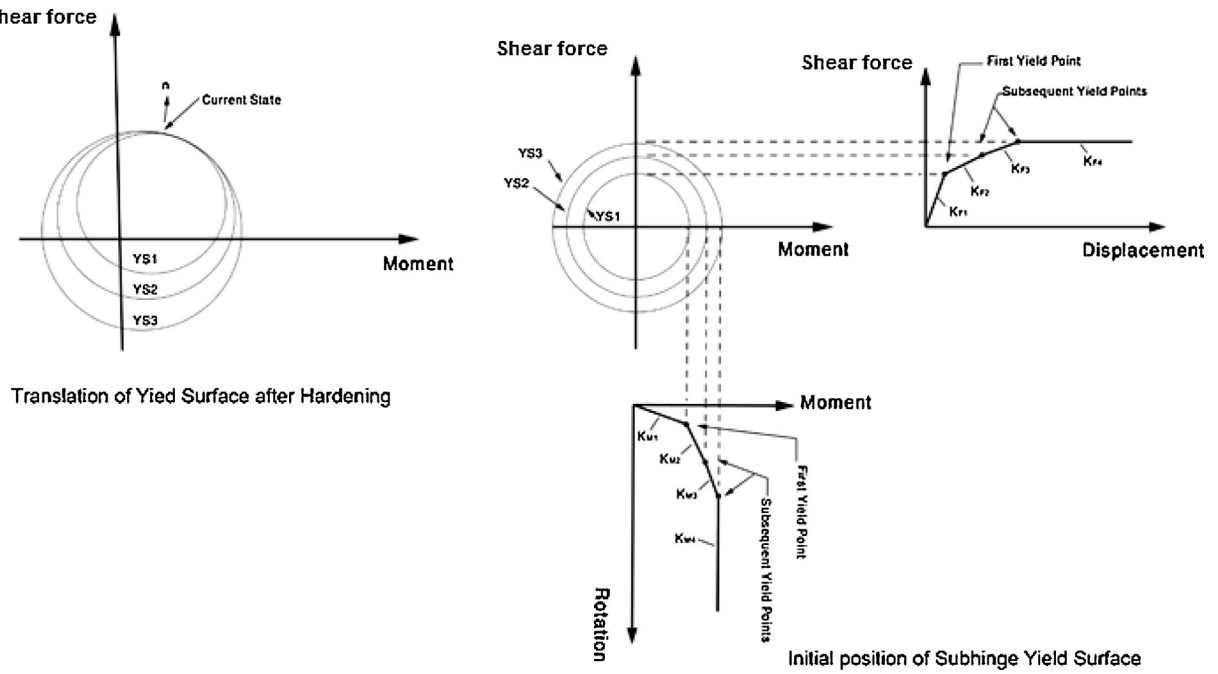


Fig. 4. Strain hardening effect.

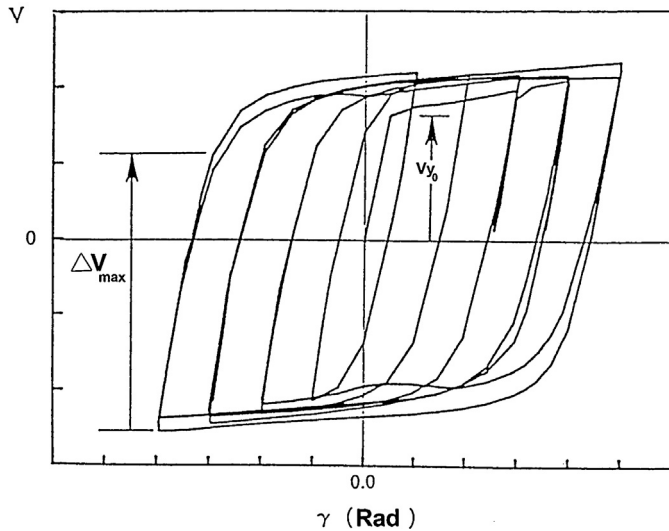


Fig. 5. Definition of the isotropic hardening parameters.

Experimental evidence suggests that there exists an upper-bound function that shows and eventually stops the increase in the shear force developed by the shear hinges. A function that represents the expansion of the yield surface due to shear yielding to account for the upper bound of shear is proposed by the Ricles and Popov [10] as following:

$$H(\varepsilon) = 0.5[\Delta V_{max} - (\Delta V_{max} - 2V_{y0}) \times e^{(-\beta\varepsilon)}] \quad (8)$$

where

V_{y0} , ΔV_{max} are initial shear yield strength and maximum shear yield strength after complete hardening, Fig. 5. ε is sum of positive plastic shear strain, β is numerical constant to be determined from a best fit of the model results with experimental measurements.

The use of Eq. (7) implies that the yield function along a horizontal facet, where Isotropic shear hardening develops, is equal to:

$$\Phi [S, \alpha, H(\varepsilon)] = \frac{V - \alpha_V}{H(\varepsilon)} = 1.0 \quad (9)$$

V = the shear force.

when

$$\partial\Phi [S, \alpha, H(\varepsilon)] > 0 \quad (10)$$

When the flexural yielding is along the vertical facet, the hardening function becomes:

$$\Phi [S, \alpha, H(\varepsilon)] = \frac{M - \alpha_M}{M_y} = 1.0 \quad (11)$$

where α_V and α_M are the translation of the yield surface along the shear and flexure axis, respectively.

The Kinematic hardening in a subhinge is controlled by the parameters α_V and α_M that make the component of the translation vector. In the shear link region no interaction between bending and shear yield surface has been seen [5,8,11], a rectangular yield surface can be adopted for the subhinges.

3.4. Determination of plastic stiffness

The plastic stiffness matrix $\underline{\underline{K}}_{spi}$ for each subhinge is:

$$\underline{\underline{K}}_{spi} = \begin{bmatrix} K_{pMi} & 0 \\ 0 & K_{pVi} \end{bmatrix} \quad (12)$$

The selection of the shear stiffness K_{pVi} of subhinge i is determined by adding the elastic beam shear flexibility to the yielded subhinge flexibility. It can be shown that when the subhinge 1 yields, $V_{y1} \leq V < V_{y2}$ then the flexibility matrix is equal to:

$$\frac{1}{K_{V2}} = \frac{1}{K_{V1}} + \frac{1}{K_{pVi}} \quad (13)$$

Thus

$$K_{pVi} = \frac{K_{V1} \times K_{V2}}{K_{V1} - K_{V2}} \quad (14)$$

When the subhinge i yields, $V_{yi} \leq V < V_{yi+1}$, the flexibility matrix becomes:

$$\frac{1}{K_{Vi+1}} = \frac{1}{K_{V1}} + \sum_{j=1}^i \frac{1}{K_{pVi}} \quad (15)$$

and

$$K_{pVi} = \frac{K_{Vi} \times K_{Vi+1}}{K_{Vi} - K_{Vi+1}} \quad (16)$$

In general case, the plastic stiffness coefficient K_{psi} for subhinge i with the action S (shear force or moment) is defined as; $S_{yi} \leq S < S_{yi+1}$ and:

$$K_{psi} = \frac{K_{Si} \times K_{Si+1}}{K_{Si} - K_{Si+1}} \quad (17)$$

4. Experimental study

4.1. Experimental specimens and test setup

Three specimens were prepared and tested to evaluate behavior of V-EBF system. The specimens were designed to yield primarily in shear. To avoid lateral buckling at both end and middle of the floor beam, later restraint was provided. Fig. 6 shows the schematic of the experimental model and test setup. The test setup, the columns and diagonal braces, respectively, were constructed from two][UPN140 and two][UPN220 profiles (for three specimens) with hinged end connection. The St37 steel having 240 MPa yield strength was used for steel materials. The properties of shear links and beam floor are listed in Table 1.

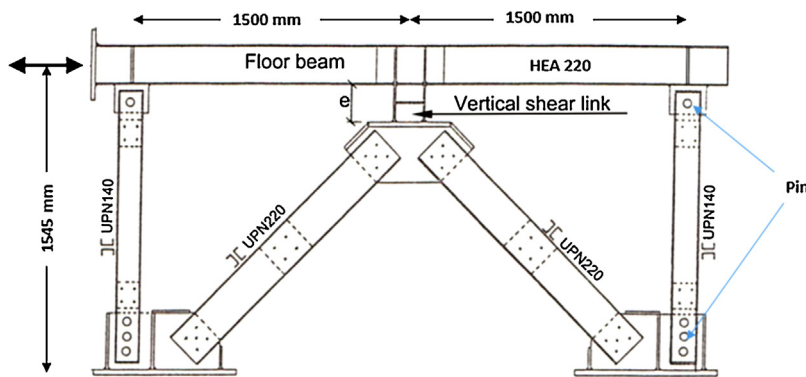


Fig. 6. Test frame using to detailed test.

Table 1
Specimen properties.

Specimen	Floor beam	Vertical shear link	e (mm)
No. 1	HEA-220	HEA-180	200
No. 2	HEA-280	HEA-240	250
No. 3	HEA-320	HEA-280	300

Table 2
Characters of strength results.

Specimen	V _p (kN)	M _p (kNm)	Testing results			
			V _y (kN)	V _u (kN)	γ _u (rad)	M _{bot} /M _{top}
No. 1	168	97.5	160	325	0.07	2.7
No. 2	280	223.5	260	570	0.072	1.06
No. 3	299	333.6	290	600	0.113	0.81

M_{bot}/M_{top} at the yielding of the link web.

The instrumentation of the specimen was designed to permit the test control, the recording of global structural response and local elements especially in the critical region such as vertical shear link region. Displacement gauges (LVDS) and strain gauges (SG) with special cable shield transferred data obtained from specimens (selected regions) to data logger.

4.2. Loading program

All specimens were subjected to quasi static cyclic with slowly displacement controlled loading to determine the cyclic load-displacement characteristics of each vertical shear link. The loading was in plane of the link's web.

A loading history was used, that cyclic displacement increased until failure of the shear link. First a few linear cyclic were performed to check the instrumentation and then to find a cyclic near the expected yield displacement. The next cycle began the incremental portion of the loading history. Two cycles were performed at displacement level of ±1.5 mm, ±2.0, ±3.0, ±3.5, ±4.0, ±5.0, ±6, ±7, ±8, ±9, ±10, ±12, ±14, ±16, ±18, ±20, ±22, ±24, ..., until failure of the shear link.

5. Discussion and results

In this section, experimental data obtained from the tests is presented and the general behavior from a practical or design point of view will be discussed. It should be noted that occurrence of the yielding on specimen is based on the observed flaking of whitewash painted on the link region and study of the monitored hysteretic loops of the shear link during the test. The general behavior of each specimen is link shear force (V) versus link rotation (γ) that the rotation γ is defined as relative end deflection of the link divided by the link length e (Fig. 2).

5.1. Strength

The load corresponding to initial yielding, ultimate strength (when the tearing of material has occurred) of the specimens are listed in Table 2. In the all specimens, real shear yielding was occurred 5%, 6% and 7% for specimens 1, 2 and 3, respectively below the theoretical V_p values of shear yielding.

As mentioned before, to assure desirable performance of EBF system after designing of the shear link, the elements outside the link are designed to resist forces generated by the fully yielded and strain hardened link. According to AISC

Table 3

Experimental results of deformation and ductility.

No. 1	1.5	0.0075	14	0.07	9.33
No. 2	2.5	0.01	18	0.072	7.2
No. 3	4	0.013	34	0.113	8.5
Specimen	Δy (mm)	γ_y (rad)	Δu (mm)	γ_u (rad)	Ductility ratio

Note: Ductility ratio = Maximum displacement divided by yielding displacement.

[23] the generated forces can be calculated as $1.25R_yV_n$ ($V_n = 0.6A_w \times F_{yw}$) to predict maximum expected shear forces. The ultimate strength of the shear link in all experimental specimens were over 200% greater than the yielding strength. To assure the good performance of V-EBF systems, it is suggested that it be used 1.75 instead of the 1.25 to predict maximum expected shear strength of shear link. The increased factor 1.75, include also the actual shear yielding comparing the theoretical values.

Based on the above, the following formula is suggested to develop the ultimate shear force up to $2.0V_p$ and maximum possible end moments in the vertical shear links without any failure at both ends of link. So, the classification of the V-EBF is modified as follows:

$$e \leq \frac{2 \times 1.2M_p}{2V_p} = 1.20 \frac{M_p}{V_p} \quad (18)$$

5.2. Two end moment of links

In the specimen 1 and 2 minor yielding was appeared at the bottom end of the flange links during cycles $\pm 5\text{mm}$ but in specimen 3 no significant flange yielding was apparent till to web buckling. In specimen 3, at first cycle of $\pm 32\text{ mm}$ displacement the link web buckled when the link rotation was $\gamma = 0.105\text{ rad}$, failure occurred in cycle $\pm 34\text{ mm}$ by tearing originating at the web-flange junction. During this cycle the tearing took place around the perimeter of the shear link. The moment versus rotation at two end of the vertical shear link obtained specimen tested is shown in Fig. 7. Results indicate that the vertical links have a stable hysteresis loops. But moments at two ends have different values. At the shear yielding of the link web, the ratio of the moment of the bottom and upper end is shown in Table 2. The end stiffness effects have to be considered in determining the length of the vertical link. With elastic link end moment and the conception consideration reflected in Eq. (19), the following design condition for link length could be specified:

$$e \leq 0.35(K+1) \frac{M_p}{V_p} \quad (19)$$

where the K factor is ratio of the moment at floor-beam divide to moment at end bottom ($0 \leq K \leq 1$). To accommodate large shear distribution in the web and prevent weld failure at the interface between link and floor beam, it is proposed to limit the moment at the upper end of the vertical link effectively to an elastic design moment of 0.5 Mp .

5.3. Deformability and energy distribution

Figs. 8 and 9 show the hysteresis behavior of the experimental specimen studied. Based on these figures, all specimens are able to dissipate the energy with stable hysteresis loops (without any pinching till failure), especially Specimen 3. Comparison of the hysteresis curves show that performance of the vertical shear links govern the system in all specimens that proves the vertical shear link act as ductile fuse to absorb energy. Also, the V-EBFs showed a ductile system against lateral load, the ductility ratio is listed in Table 3.

5.4. Corrective of analytical model

5.4.1. Analytical modeling

The Drain-2DX program with the developed shear link element was used to perform nonlinear analysis of the V-EBF system. Each shear link element was modeled as a two dimension element. The degrees of freedom of the shear link are defined in horizontal, vertical and rotational direction at both ends. Both Kinematic and Isotropic strain hardening were considered for shear and their degrees of participation were empirically assigned. Also, only the Kinematic hardening effect was considered for moment. The shear link elements have the same mathematical idealization and assumption according to part 3.

5.4.2. Comparison of analytical & experimental results

The local (vertical shear link) and global (general response of the test frame) hysteresis response curves for the three specimens tested to compare with analytical models are shown in Fig. 10. Results indicate that the elastic stiffness of the analytical model is good agreement with the measured value for the specimens. The combine Isotropic and Kinematic hardening behavior of the model also correlates well with the experimental behavior. Furthermore, the model predicts shear yielding in the vertical links were approximately.

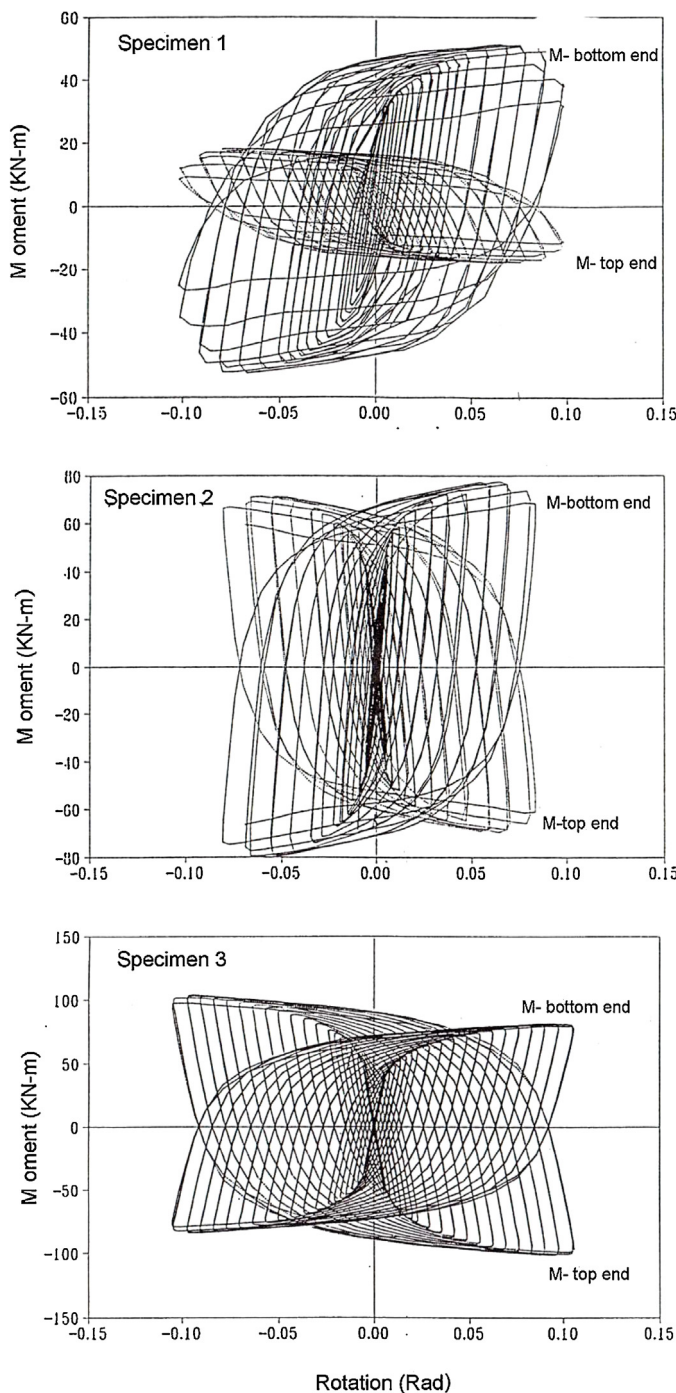


Fig. 7. Links ends moment-rotation response.

The comparison of the shear responses of analytical model and the test results show that they cover each other 95% approximately in local and global responses. It means that the vertical shear link model is capable to predict cyclic response of the V-EBF in local and global responses.

Considering Section 3.3, the function that represents the expansion of yield surface (strain hardening) due to shear yielding to account for upper bound of shear is developed. The function determines the maximum attainable shear force

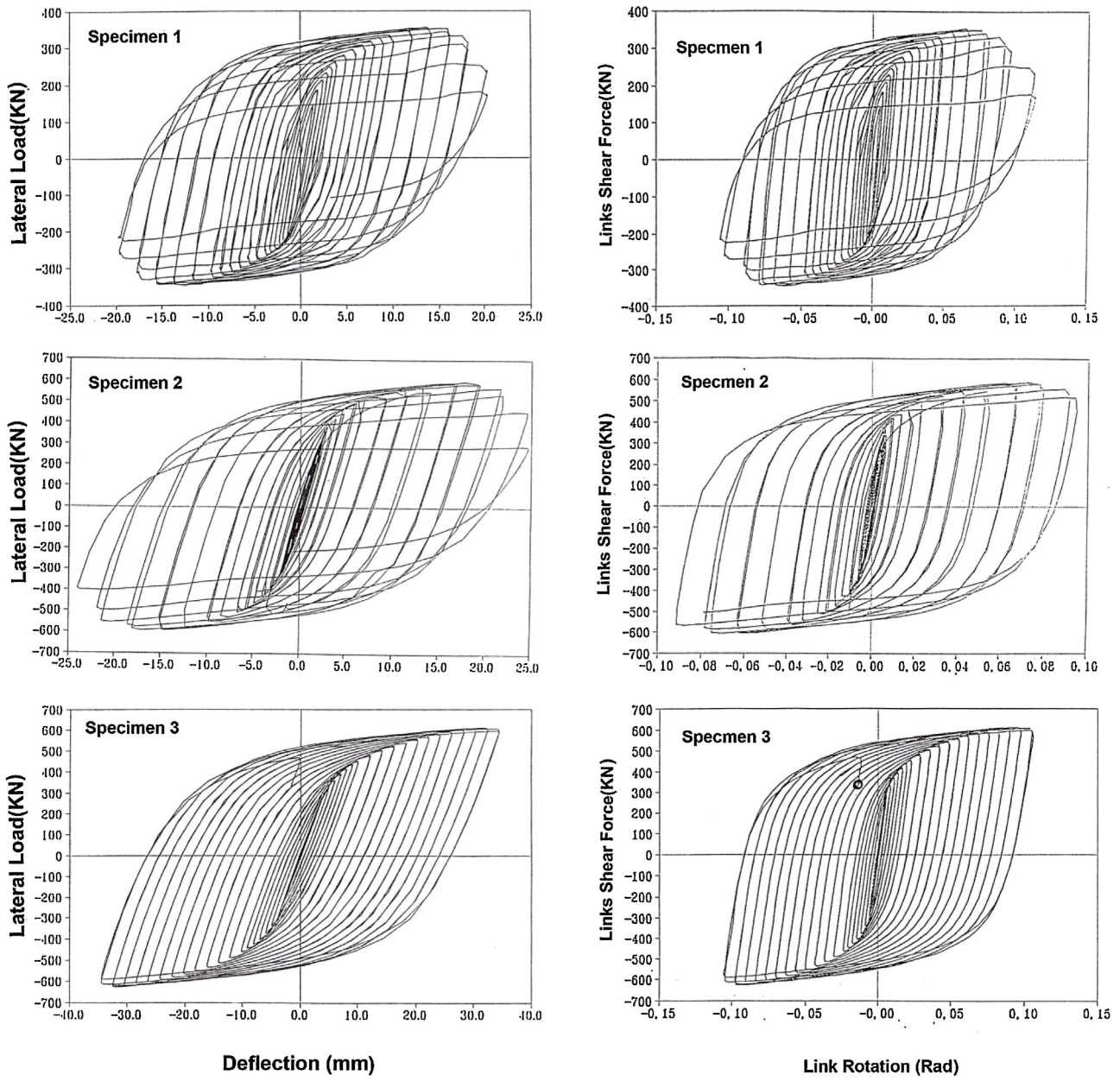


Fig. 8. Hysteresis curves of experimental models.

(V_{ISO-h}) after certain amount of plastic deformation has occurred. Based on the experimental results, model calibration in part 3.5, the following function shape is proposed for expansion of shear yield surface or Isotropic hardening:

$$V_{ISO-h} = 2.15V_y - 1.15V_y \times e(-6\sum\gamma_p) \quad (20)$$

All parameters have defined previously.

The proposed equation agrees with experimental results and provides an upper bound for the Isotropic hardening of the yielding surface of the vertical link under cyclic loading, Fig. 11.

5.5. Model calibration for vertical link

Based on the experimental results and analytical study in this paper, the indicated force-deformation relationship is proposed. The multi-linear values governing the shear force-deformation and bending moment-rotation relationships shown in Fig. 3 were calibrated based on the test results. In comparing with the horizontal shear link, the numerical formulation of

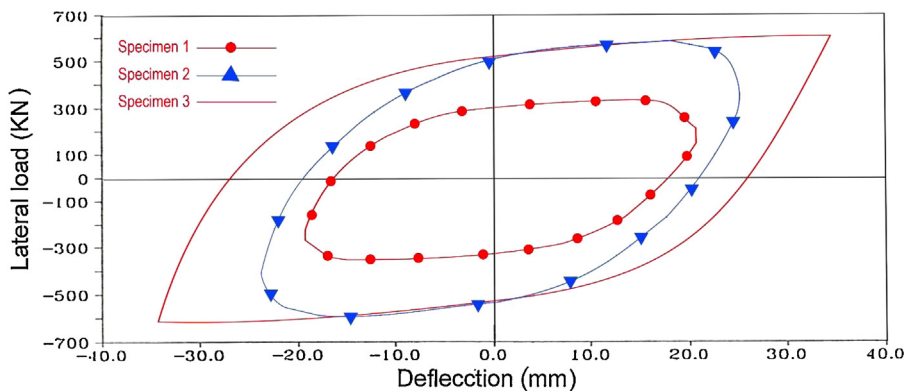


Fig. 9. Comparison of envelop of hysteresis loops.

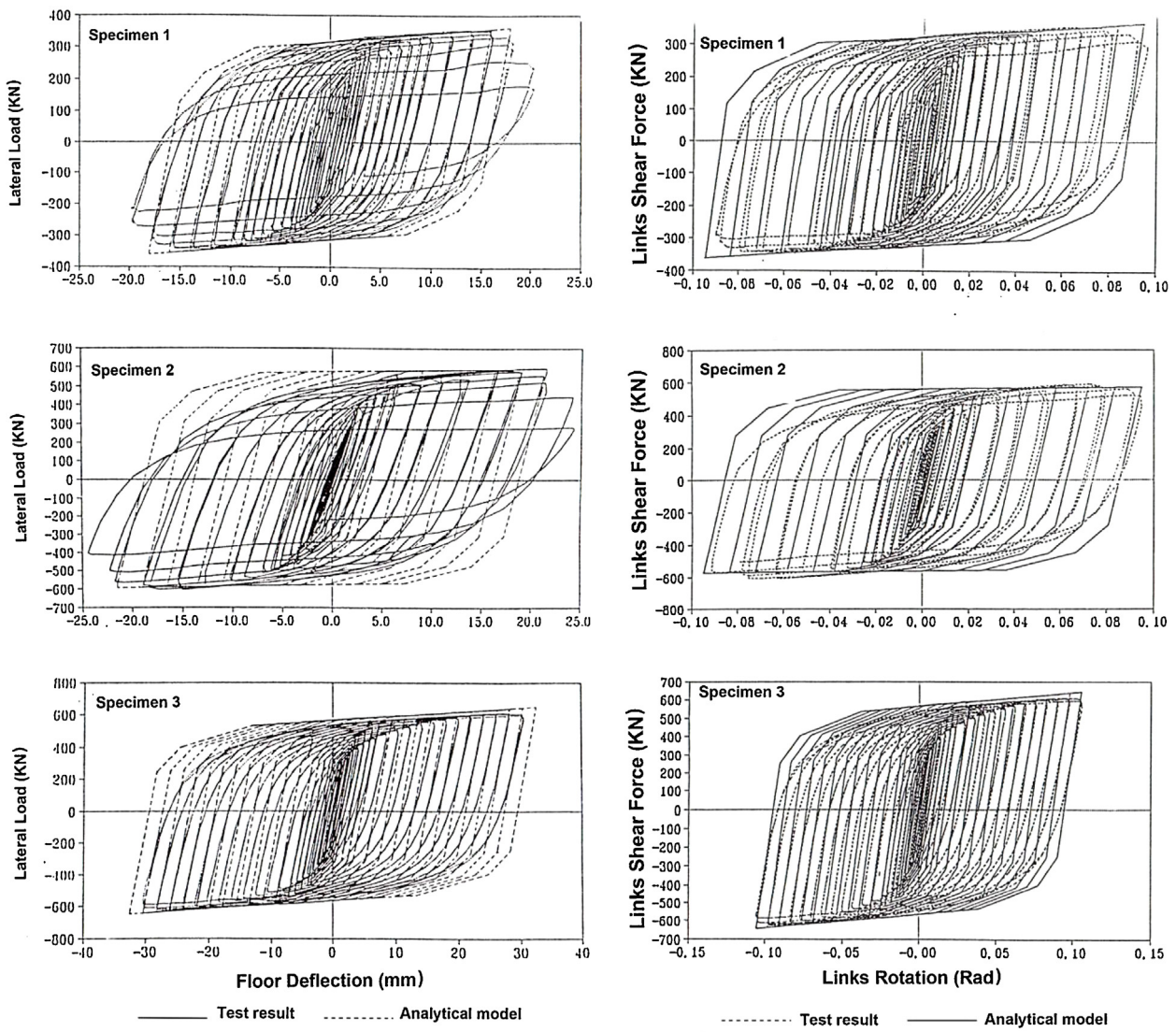


Fig. 10. Comparison of the experimental & analytical results.

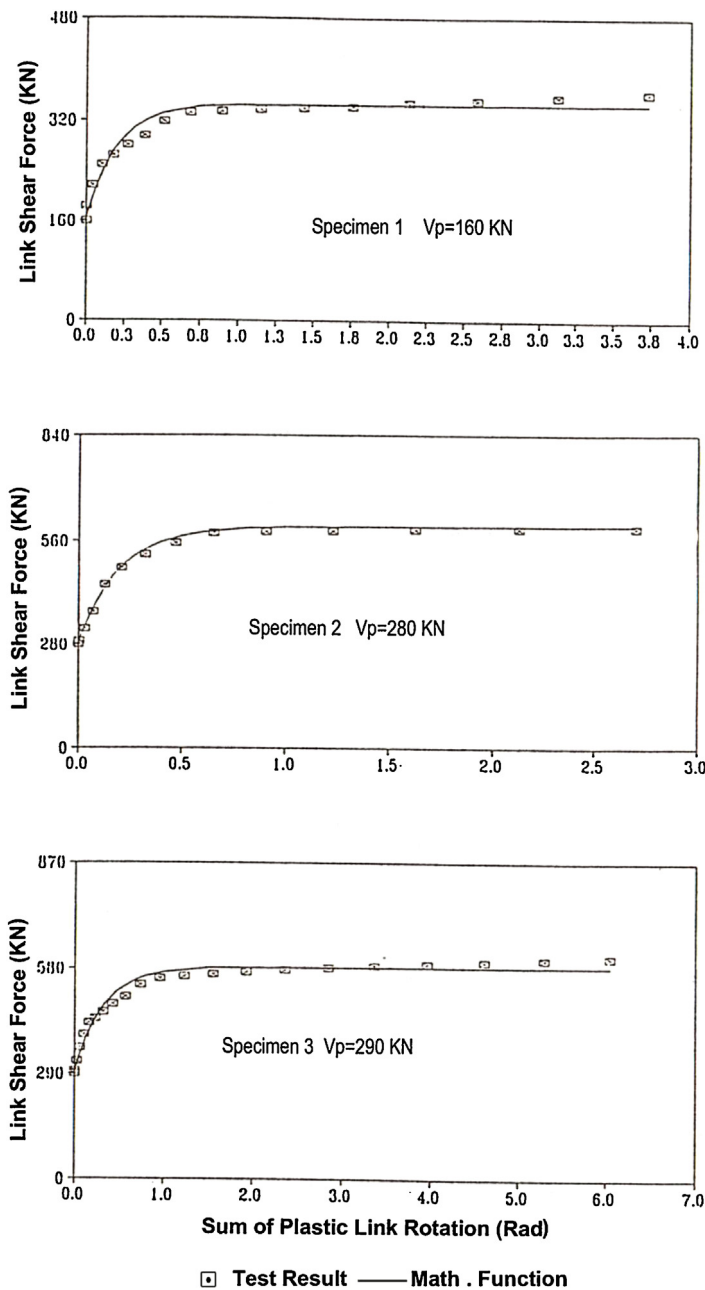


Fig. 11. The isotropic hardening of experimental and mathematical shear expansion.

the shear and moment stiffness calibration factors for vertical shear link have been formulated as following characteristic values:

$$V_{y1} = 1.00V_y \quad M_{y1} = 1.00M_y$$

$$V_{y2} = 1.50V_y \quad M_{y2} = 1.03M_y$$

$$V_{y3} = 2.00V_y \quad M_{y3} = 1.06M_y$$

$$K_{V2} = 0.100K_{V1} \quad K_{M2} = 0.030K_{M1}$$

$$K_{V3} = 0.030K_{V1} \quad K_{M3} = 0.015K_{M1}$$

$$K_{V4} = 0.007K_{V1} \quad K_{M4} = 0.002K_{M1}$$

where

$$K_{M1} = \frac{3EI}{e}; \quad K_{V1} = \frac{GA_w}{e}$$

Bending moments at the two end of a V-EBF are different despite of horizontal EBF (bending moments at the two end of the horizontal EBF are equal). Because of this difference, the stiffness calibration factors for vertical shear link and horizontal shear link (formula obtained from Section 3.2) are different.

6. Conclusions

From the study of theoretical and experimental results the following major conclusion can be derived:

- The V-EBF indicated a ductile system (with high ductility ratio) that is able to dissipate the energy with stable hysteresis loops (without any pinching till failure).
- Experimental results showed that inelastic deformation is confined in vertical link and its performance governs on the system in all specimens. This occurrence proves that the vertical shear link act as ductile fuse to absorb energy. It is possible to find an upper bound of maximum strength of V-EBF.
- Shear yielding (V_p) in the experimental testing was occurred 5–7% below the force at the theoretical values, also, ultimate strength of the shear links reached up to $2V_p$. So, the length of vertical link should be limited to $2V_p$.
- The ends stiffness effects have to be considered in determining the length of the vertical link. It is proposed to limit the moment at the upper end of the vertical link effectively to an elastic design moment of 0.5 MPa.
- Analytical model showed a good convergence with experimental results in local and global responses. It means that the vertical shear link model is capable of predicting reasonably well the cyclic response of V-EBF in local and global responses.
- The combine Isotropic and Kinematic hardening behavior of the analytical model correlates well with the experimental behavior. Furthermore, the model predicts shear yielding in the vertical links were approximately.
- Considering the anisotropic rule, that assumes Isotropic-Kinematic hardening in shear yielding, and only Kinematic hardening for moment yielding, the yield function provides an upper bound for the Isotropic hardening of the yielding surface of the vertical link under cyclic loading.

Acknowledgment

This study was supported by IIEES. The main fund was about vertical shear link project that have been performed in IIEES.

References

- [1] C.W. Roeder, E.P. Popov, Eccentrically braced steel frames for earthquakes, *J. Struct. Div.* 104 (1987) 391–412.
- [2] C.W. Roeder, E.P. Popov, Cyclic shear yielding of wide-flange beams, *J. Eng. Mech. Div.* 104 (1987) 763–780.
- [3] E.P. Popov, W. Bertero, Seismic analysis of some steel building frames, *J. Eng. Mech. Div.* 106 (1980) 75–92.
- [4] K.D. Hjelmstad, E.P. Popov, Cyclic behavior and design of link beams, *J. Struct. Eng.* 109 (1983) 2387–2403.
- [5] K.D. Hjelmstad, E.P. Popov, Seismic Behavior of Active Links in Eccentrically Braced Frame, Report No. UCB/EER-83/15, Berkeley, California, 1983.
- [6] J. Malley, E.P. Popov, Shear links in eccentrically braced frames, *J. Struct. Eng.* 110 (1984) 2275–2295.
- [7] J. Malley, K.D. Hjelmstad, E.P. Popov, Design Consideration for Shear Link in Eccentrically Braced Frames, Report No. UCB/EER-83/24, Berkeley, California, 1983.
- [8] K. Kasai, E.P. Popov, Study of Seismically Resistant Eccentrically Braced Steel Frame Systems, Report no. UCB/EERC-86/01, Earthquake Engineering Research Center, 1986.
- [9] E.P. Popov, M.D. Engelhardt, Seismic eccentrically braced frames, *J. Constr. Steel Res.* 10 (2016) 321–354.
- [10] J.M. Ricles, E.P. Popov, Dynamic Analysis of Seismically Resistant Eccentrically Braced Frames, Report No. UCB/EERC-87/07, Earthquake Engineering Research Center, University of California, Berkeley, CA, 1987.
- [11] J.M. Ricles, E.P. Popov, Experiments on Eccentrically Braced Frames with Composite Floors, Report No. 87/06, Earthquake Engineering Research Center, University of California, Berkeley, 1987.
- [12] M.D. Engelhardt, E.P. Popov, Experimental performance of long links in eccentrically braced frames, *J. Struct. Eng.* 118 (1992) 3067–3088.
- [13] J.D. Aristizabal-Ochoa, Disposable knee bracing: improvement in seismic design of steel frames, *J. Struct. Eng.* 112 (1986) 1544–1552.
- [14] A. Ghobarah, H. Abou-Elfath, Rehabilitation of a reinforced concrete frame using eccentric steel bracing, *Eng. Struct.* 23 (2001) 745–755.
- [15] M. Vetr, N. Shirali, A. Ghamari, Seismic resistance of hybrid shear wall (HSW) systems, *J. Constr. Steel Res.* 116 (2016) 247–270.
- [16] S.M. Zahrai, M. Bruneau, Cyclic testing of ductile end-diaphragms for slab-on-girder steel bridges, *J. Struct. Eng. ASCE* 125 (1999) 987–996.
- [17] P. Dusicka, A.M. Itani, I.G. Buckle, Cyclic behavior of shear links and tower shaft assembly of San Francisco–Oakland Bay bridge tower Technical Report-CCEER 02-06, Center for Civil Engineering Earthquake Research, 2002.
- [18] J.W. Berman, M. Bruneau, Supplemental system retrofit considerations for braced steel bridge piers, *J. Earthq. Eng. Struct. Dyn.* 34 (2005) 497–517.
- [19] J.W. Berman, M. Bruneau, Approaches for the seismic retrofit of braced steel bridge piers and proof-of-concept testing of a laterally stable eccentrically braced frame Technical Report-MCEER-05-0004, Multidisciplinary Center for Earthquake Engineering Research, 2005.
- [20] J.G. Bouwkamp, M. Vetr, Design of eccentrically braced test frame with vertical shear links, in: Proceedings of the 2nd International Conference on Earthquake Resistant Construction and Design, Berlin, 1994.
- [21] M. Vetr, M. Shayanfar, M. Barkhordari, A. Rezaeian, Seismic behavior of eccentrically braced frames with composite vertical shear link, *J. Iran. Soc. Steel Struct.* (2011), In Persian Language.

- [22] S.H. Chao, C.G. Subhash, Performance-Based Seismic Design of EBF Using Target Drift and Yield Mechanism as Performance Criteria, Research Report-UMCEE 05-05, Department of Civil and Environmental Engineering University of Michigan, 2016.
- [23] AISC, Seismic provisions for structural steel buildings, AISC, Chicago, 2010.
- [24] K. Young, H. Adeli, Fundamental period of irregular eccentrically braced tall steel frame structures, *J. Constr. Steel Res.* 120 (2016) 199–205.
- [25] T. Ramadan, A. Ghobarah, Analytical model for shear-link behavior, *J. Struct. Eng. ASCE* 121 (1995) 1574–1580.
- [26] Z. Morz, On the description of anisotropic workhardening, *J. Mech. Phys. Solids* 15 (1967).
- [27] Z. Morz, An attempt to describe the behavior of metal under cyclic loads using a more general workhardening, *Acta Mech.* 7 (1969).